Structure and Dynamics of Liquid Crystalline Pattern Formation in Drying Droplets of DNA

Ivan I. Smalyukh,[1,2] Olena V. Zribi,[1] John C. Butler,[1] Oleg D. Lavrentovich,[2] and Gerard C. L. Wong[1,*]

[1]*Department of Physics, Department of Materials Science and Engineering, Department of Bioengineering, University of Illinois at Urbana-Champaign, Urbana, Illinois 61801, USA*

[2]*Liquid Crystal Institute and Chemical Physics Interdisciplinary Program, Kent State University, Kent, Ohio 44242, USA*

(Received 1 January 2006; published 2 May 2006)

We investigate the formation of ringlike deposits in drying drops of DNA. In analogy with the colloidal ''coffee rings,'' DNA is transported to the perimeter by the capillary flow. At the droplet edge, however, DNA forms a lyotropic liquid crystal (LC) with concentric chain orientations to minimize the LC elastic energy. During the final stages of drying, the contact line retracts, and the radial stress causes undulations at the rim that propagate inward through the LC and form a periodic zigzag structure. We examine the phenomenon in terms of a simple model based on LC elasticity.

DOI: 10.1103/PhysRevLett.96.177801 PACS numbers: 61.30.Pq, 61.30.Vx, 81.16.Fg, 87.14.Gg

Drying droplets of colloidal suspensions form ''coffee ring'' stains due to the capillary flow caused by contact line (CL) pinning [1]. This phenomenon has been used for the assembly of nanoparticles [2,3] and diblock copolymers [4]. For gene expression profiling, an array of DNA droplets is often dried on a glass surface for hybridization studies [5]. Since DNA can be stretched by flow [6–9] and ''molecular combing'' [10], single DNA chains usually align *perpendicular* to the CL of a drying drop. In this Letter, we show that, when a concentrated DNA droplet is dried, a coffee ring stain is also formed, but, contrary to intuition, the extended DNA chains trace out zigzags *along* the CL and form a periodic pattern (Fig. 1). During most of the drying time, the contact line is pinned, and DNA chains from the droplet interior are transported to the perimeter. At the droplet edge, a lyotropic liquid crystal (LC) is formed, in which DNA chains align along the droplet edge to minimize LC elastic and surface anchoring energies. During the final stages of drying, the CL retracts, and radial dilative stress causes undulations at the rim that propagate inward through the elastic LC medium, giving rise to the domain pattern. A simple model based on LC elasticity explains the observations.

The experiments are conducted using λ-DNA (contour length $l_c \approx 16.3$ μm, 48 502 bp, persistence length $l_p \approx 50$ nm), obtained from New England BioLabs, Inc. The pattern is observed for a broad range of initial DNA concentrations $C_i = (0.02–5)$ mg/ml, initial droplet volumes $V_i = (1–50)$ μl, and for surfaces with different hydrophilicity (clean glass plates, SiO, and indium tin oxide coatings, etc.; contact angle $15° \leq \alpha \leq 110°$). The droplet's radius $R = (0.5–12)$ mm is varied by changing V_i and α. The pattern consists of the herringbonelike domains with a self-similar periodic structure (Fig. 1). The periodicity L and deposit thickness d increase with V_i and C_i; in the deposits, L is a monotonously increasing function of d [Fig. 1(a)], measured using confocal microscopy vertical cross sections [Fig. 1(f)]. For example, L can be varied from $L < l_c$ to $L > l_c$ and d from submicron to tens of microns by changing $V_i = (1–50)$ μl [Fig. 1(a)]. For DNA rings of $d < 10$ μm obtained with droplets of $V_i < 30$ μl at 1 mg/ml of DNA, the polarizing microscopy (PM) textures appear gray [Fig. 1(c)]. PM images are polychromatic if $V_i \geq 30$ μl [Fig. 1(d)], indicating that, for wavelengths λ in the visible spectral range, $\Delta n d \sim \lambda$, where $\Delta n = n_e - n_0$ and n_e, n_0 are extraordinary and ordinary refractive indices. We estimate Δn by correlating texture colors and the measured d: $\Delta n = -0.011 \pm 0.004$ for a

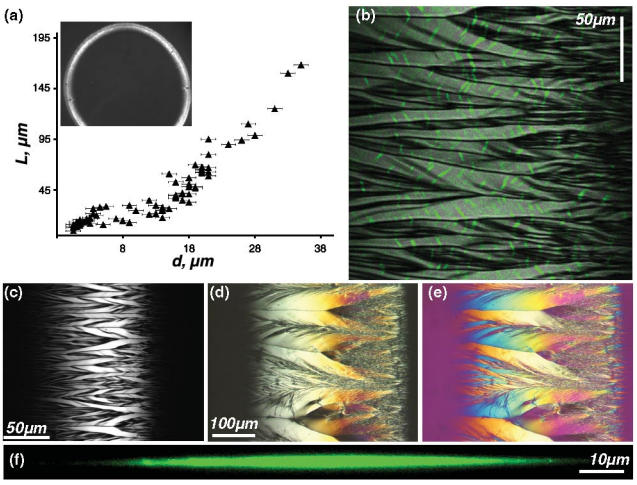

FIG. 1 (color). DNA pattern at the perimeter of a dried drop: (a) periodicity L vs thickness d in the central thickest part of the ring [obtained by varying $V_i = (1–50)$ μl]; the inset shows a typical birefringent ring; (b) PM texture of the pattern colocalized with the fluorescence signal from a small number of molecules marked by YOYO-1; (c)–(e) PM textures of the pattern inside (c) a thin (<10 μm) ring and (d),(e) a thick (>20 μm) ring obtained (c),(d) without and (e) with a 530 nm retardation plate; (f) a vertical confocal microscopy cross section (all DNA labeled) showing the bell-shaped profile of the ring. The crossed polarizer and analyzer are parallel to the vertical and horizontal directions in the plane of the images in (a)–(e), and the retardation plate is at 45° to them in (e). The CL is on the right side of the ring fragments in (b)–(f).

dried film of λ-DNA ($\Delta n < 0$ because of the conjugated bonds in base pairs) and even smaller in the lyotropic LC observed during drying. Droplets of $V_i < 1$ μl, such as those in DNA chips, also produce ringlike deposits, but the pattern is barely observable in PM because Δnd is small.

The PM texture of the pattern (Fig. 1) changes upon rotation of the sample; each part can be brought to extinction at a well-defined orientation with respect to the crossed polarizers. This indicates that the director $\hat{n}$ (average local orientation of DNA chains) is not twisted along the normal to the substrate, in agreement with the theoretical predictions [11] that twist is suppressed with increasing the polymer contour length and in phases with positional order. When the sample is rotated in the presence of a 530 nm retardation plate between crossed polarizers, continuous changes of alternating blue and orange bands are observed [Fig. 1(e)]. This allows one to deduce the thickness-averaged in-plane $\hat{n}$. The result agrees well with the fluorescence signal from the dyed DNA molecules within unlabeled DNA [12] colocalized with the PM texture [Fig. 1(b)]: The extended DNA and $\hat{n}$ are uniformly oriented at $\pm(30°–45°)$ to the CL within the stripes and the in-plane $\hat{n}$ traces out zigzags from stripe to stripe.

In order to elucidate the 3D structure of $\hat{n}(x, y, z)$, we use fluorescence confocal polarizing microscopy (FCPM) [13] and stain the DNA with acridine orange dye (AO, Aldrich Chemical Co.), which intercalates parallel to the base pairs [14], i.e., approximately perpendicular to the DNA axis (Fig. 2). When studied with polarized FCPM light, the spatial pattern of fluorescence signal visualizes the director structure [15]. To resolve $\hat{n}$ across the film thickness, we study thick, $d = (20–50)$ μm, deposit rings obtained after drying of droplets of $V_i \approx 50$ μl at (1–2) mg/ml of DNA. The FCPM resolution (≈ 1 μm) is sufficient to resolve the structure of $\hat{n}$ in 3D: The pattern is composed of stripes with essentially thickness-independent periodically alternating $\hat{n}$ parallel to the substrate and at $\pm(45°–60°)$ to the radial direction (Fig. 2). The vertical wall defects run across the whole thickness of the ring [Figs. 2(e)–2(h)] and are due to the discontinuous jumps of $\hat{n}$ between the stripes.

To get insights into the physics of this phenomenon, we experimentally study dynamics of the droplet drying. At the initial stages, it resembles coffee ring formation [1]. As long as the CL is pinned (Fig. 3), the evaporation flux is the strongest next to the edge of the drop. As evidenced by tracking fluorescently labeled tracer DNA, the solute flows from the drop interior toward the periphery to compensate the evaporation losses. This radial outward flow transports random-coiled DNA (~ 1 μm globules) to the drop's perimeter. DNA concentration at the perimeter and the local effective viscosity gradually increase so that DNA Brownian motion is hindered (as observed by tracking fluorescently dyed molecules). The Stokes drag becomes strong enough to extend DNA [7–9], driving the LC self-

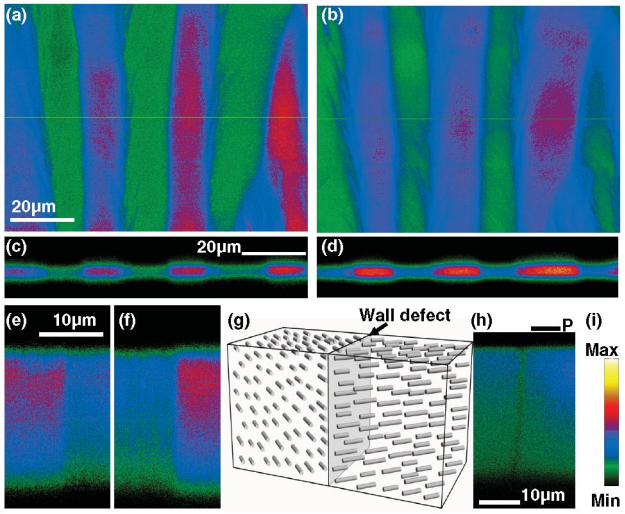

FIG. 2 (color). (a),(b) In-plane and (c),(d) vertical FCPM cross sections of the director structure in a relatively thin ring; (e),(f) vertical FCPM cross sections obtained for a thick ring illustrating that orientation of $\hat{n}$ across the film thickness is the same within the stripes; (g) schematics of DNA orientation (visualized by cylinders) in domains with $\hat{n}$ at $\approx \pm 45°$ to the radial direction and the vertical wall defect (shaded plane) in between; (h) a typical FCPM vertical cross section of a thick ring (FCPM polarization along the local CL) visualizes the wall defect separating domains with nearly orthogonal $\hat{n}$; (i) FCPM intensity scale. The polarization of the FCPM probing light is at $-45°$ with respect to the radial direction in (a),(c),(e) and at 45° in (b),(d),(f).

organization at the droplet rim [16]. The drop at this stage has a birefringent wedge-shaped LC ring with $\hat{n}$ parallel to the CL, which is still pinned at the initial location. The DNA alignment parallel to the drop's edge is counterintuitive because DNA is expected to extend along the flow [7–9], which is mainly in the radial direction. To understand these experimental observations, we consider the LC surface anchoring and bulk elastic properties [11,16–21]. Although long DNA chains usually have random coil conformations, it has been demonstrated that "molecular crowding" can straighten the random coils and lead to LC phases [16]. The macroscopic elasticity can be described in a framework similar to other polymer LCs composed of long flexible chains [11,16–21]. The elastic distortions of the LC director $\hat{n}$ are associated with free energy density [20,21]:

$$f = \frac{K_1}{2}(\nabla \cdot \hat{n})^2 + \frac{K_2}{2}(\hat{n} \cdot (\nabla \times \hat{n}))^2 + \frac{K_3}{2}(\hat{n} \times (\nabla \times \hat{n}))^2 + \frac{E}{2}\frac{\delta\rho_p}{\rho_p^0}. \quad (1)$$

Here K_1, K_2, and K_3 are Frank elastic constants for splay, twist, and bend deformations of $\hat{n}$, respectively, $\delta\rho_p$ is variation of the local polymer density, ρ_p^0 is the mean polymer density, and E is the osmotic compressibility

modulus. As compared to the small-molecule LCs, the fundamental difference is that $K_1 \gg K_2, K_3$ and that there is a free energy cost for locally compressing/dilating the LC composed of long flexible chains, described by the last term in (1).

We determined that the droplet-air and droplet-substrate interfaces impose tangential boundary conditions, setting $\hat{n}$ parallel to these interfaces [22]. Satisfying these conditions, the radial structure of $\hat{n}$ would then require splay deformations of $\hat{n}$. In the limit of small α and for typical widths of the LC wedge $\Delta R \leq R/10$ [23], the associated elastic energy of the LC wedge at the perimeter is $F_{\text{radial}} \approx 10\pi\alpha K_1 R$. In contrast, the concentric structure with DNA along the CL involves bend deformations of $\hat{n}$ at the large length scales $\sim R$; the elastic energy is $F_{\text{conc}} = \pi\alpha K_3\{R \ln[R/(R - \Delta R)] - \Delta R\}$ [23]. For typical R and ΔR, one obtains $F_{\text{conc}}/F_{\text{radial}} \sim 10^{-4} K_3/K_1 \ll 1$; since $K_3 \ll K_1$, F_{conc} is much smaller than F_{radial}. This explains the concentric $\hat{n}$ (Figs. 3 and 4) that can persist until the end of drying and leave a deposit with annular DNA alignment if the CL does not recede (observed at $C_i > 15$ mg/ml for λ-DNA [23] or at even higher C_i for shorter DNA fragments [24]). The droplets with smaller C_i form a pattern that is a periodic distortion of the initial concentric $\hat{n}$.

The contact angle α varies due to evaporative water losses and slight decrease of surface tension [25]. When $\alpha = 2°$–$4°$, the CL is depinned and recedes [Figs. 3(a)–3(f)], similar to drops of other complex fluids [26]. The imposed stress and reverse (inward) radial flow pull the extended DNA in the radial direction [10], i.e., normal to $\hat{n}$. At very small C_i, the shrinking droplet with receding CL can stretch the single biopolymer molecule in the radial direction [6,10,27]. In our case of relatively large C_i, DNA molecules are extended along the CL and form an LC phase before the CL depinning. The minimum of LC elastic free energy corresponds to the concentric $\hat{n}$; hence, the radial dilative stress in the vicinity of the receding CL competes with the LC elasticity, resulting in a periodic distortions of $\hat{n}$ [Figs. 1, 2, and 3(g)]. Formed wavy undulations are reminiscent of the undulations induced by a dilative mechanical stress in columnar LCs [17,28]. At the onset of pattern formation, the distortions first appear next to the CL [Figs. 3(g) and 3(h)] and then expand to the whole width of the ring with concentric $\hat{n}$. The ripples of $\hat{n}$ at the CL propagate in the radial direction $n_r \propto \cos qx \times \exp[-q^2 r\sqrt{K_3/(E + q^2 K_1)}]$ and decay at the characteristic length $l_r = q^{-2}\sqrt{(E + q^2 K_1)/K_3}$ [Figs. 3(g) and 3(h)], where $q = 2\pi/L$; this is analogous to the response of a polymer nematic to a grooved surface [21]. For experimental $L = (3$–$150)$ μm and typical $\sqrt{K_3/E} = (5$–$10)$ nm [21], $E \gg q^2 K_1$, one obtains $l_r = (10$–$10\,000)$ μm, depending on L. This explains why the ripples of $\hat{n}$ occurring at the CL penetrate deep into the LC ring [Figs. 3(g) and 3(h)]. The periodic stripes eventually run across the whole width ΔR of the birefringent ring and act as a ''template'' for the deposition of remaining DNA. When the remaining water evaporates, solidification of the DNA deposit is followed by formation of defect walls and cracks, evidenced by additional sharp lines (Fig. 1) that are typical for phases with positional order. Interestingly, the final structure and the pattern of DNA orientation (Figs. 1, 2, and 4) resemble the ''sawtooth-type'' buckling instability observed at high applied stresses in LCs with partial positional order [17,28]. The sequence of pattern formation and the final director structure are summarized in Fig. 4.

In summary, we describe the periodic pattern formed in the coffee rings of DNA drops and explain it in terms of a

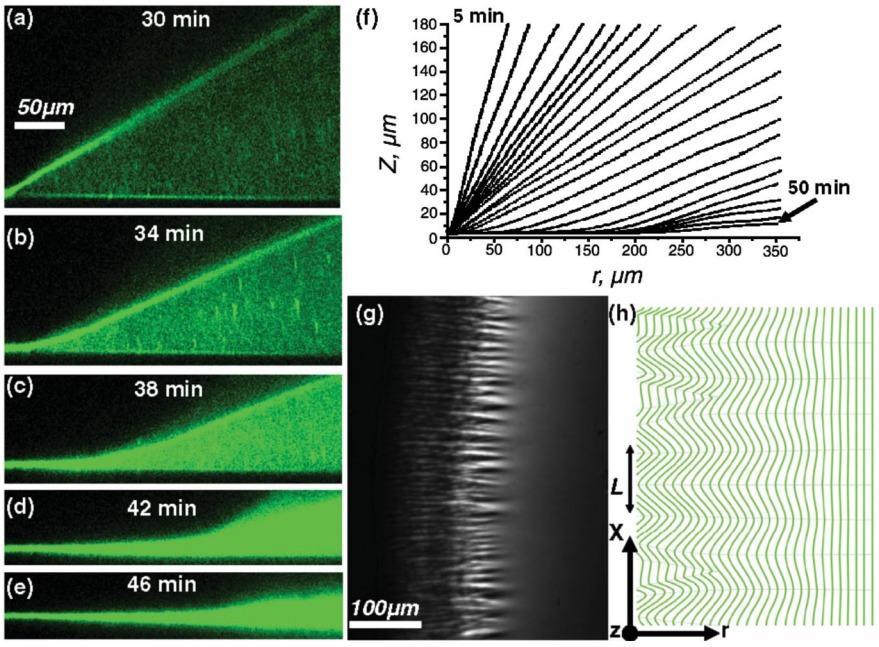

FIG. 3 (color). (a)–(e) Vertical cross sections showing drying droplet profile with (a) the CL pinned and (b)–(e) slowly receding (DNA stained with AO dye); (f) profiles of the liquid-air interface for different drying times, obtained from the cross sections similar to (a)–(e); (g) PM texture and (h) a schematic illustration showing that the periodic distortion of originally concentric $\hat{n}$ starts at the CL and propagates towards the droplet's center. The crossed polarizer and analyzer in (g) are at 30° to the vertical and horizontal directions of the PM image.

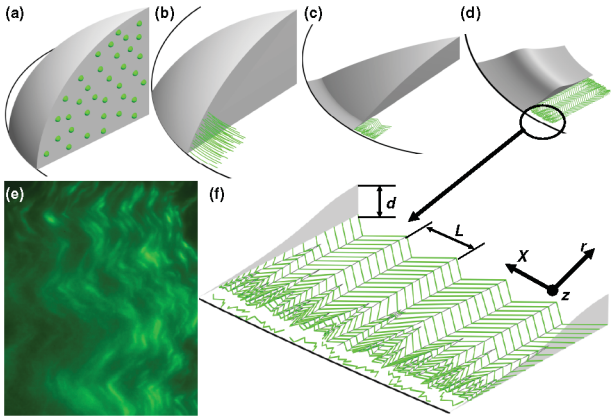

FIG. 4 (color). The sequence of pattern formation: (a) The CL is pinned and DNA is homogeneously distributed; (b) the CL is still pinned but most of the molecules have already been brought to the perimeter, stretched, and form the LC with $\hat{n}$ along the edge; (c) CL is receding and the initially concentric $\hat{n}$ undergoes undulations; (d),(e) when the drying process is complete, the DNA deposit is a bell-shaped ring (d) with the DNA zigzag pattern visualized in (e) via fluorescence from a small number of molecules stained by YOYO-1; (f) schematics of the pattern.

simple model based on the LC nature of the ring at the drying droplet edge. Similar phenomena are observed for other semiflexible biopolymers [23,29]. Questions related to details of the pattern formation remain, such as the precise mechanism of wavelength selection and the relative role of the capillary flow in the LC with viscosity coefficient anisotropy [30], as well as convection [9] and Marangoni flows [26], which modify the pattern formation at the late stages of the drying process. Since essentially all the DNA is concentrated in a narrow ring threaded by a network of defect walls with almost no DNA in the rest of the stain, these effects should be accounted for in the design of microarrays in which DNA droplets are sequentially deposited onto a surface for hybridization studies [5]. Without optimization of the wetting conditions, it is possible to damage the DNA chains or ''miss'' *all* the DNA in the ring stain of a dried droplet even if perfect center-of-mass droplet alignment is achieved.

We acknowledge discussions with J. Freund, S. Garoff, R. Larson, C. R. Safinya, J. Selinger, and J. Tang. This work was supported by the Institute for Complex and Adaptive Matter, the NSF Nanoscience and Engineering Initiative (UIUC), and the NSF Grants No. DMR-0504516 (KSU) and DMR-0409769 (UIUC).

*Corresponding author.
Electronic address: gclwong@uiuc.edu

[1] R. D. Deegan *et al.*, Nature (London) **389**, 827 (1997).
[2] E. R. Dufresne *et al.*, Phys. Rev. Lett. **91**, 224501 (2003).
[3] V. V. Tsukruk, H. Ko, and S. Peleshanko, Phys. Rev. Lett. **92**, 065502 (2004).
[4] M. Kimura *et al.*, Langmuir **19**, 9910 (2003).
[5] M. C. Pirrung, Angew. Chem., Int. Ed. **41**, 1276 (2002).
[6] M. Chopra *et al.*, J. Rheol. (N.Y.) **47**, 1111 (2003).
[7] J. F. Marko and E. D. Siggia, Science **265**, 506 (1994).
[8] T. T. Perkins, D. E. Smith, and S. Chu, Science **276**, 2016 (1997).
[9] S. S. Abramchuk *et al.*, Europhys. Lett. **55**, 294 (2001).
[10] A. Bensimon *et al.*, Science **265**, 2096 (1994); D. Bensimon *et al.*, Phys. Rev. Lett. **74**, 4754 (1995).
[11] R. D. Kamien and J. Toner, Phys. Rev. Lett. **74**, 3181 (1995).
[12] We labeled $\sim 1/10\,000$ DNA chains with dye YOYO-1 (Molecular Probes, 488 nm Ar-laser excitation and 510–550 nm fluorescence detection) so that there is one YOYO-1 molecule per 15 bp of DNA.
[13] I. I. Smalyukh, S. V. Shiyanovskii, and O. D. Lavrentovich, Chem. Phys. Lett. **336**, 88 (2001).
[14] L. S. Lerman, Proc. Natl. Acad. Sci. U.S.A. **49**, 94 (1963).
[15] AO dye (488 nm excitation and 510–550 nm detection) is doped at $(10^{-3}$–$10^{-4})$ wt. % into a 1 mg/ml aqueous DNA solution. In the used epifluorescence mode, the strongest signal corresponds to the FCPM polarization perpendicular to $\hat{n}$ and the weakest signal when it is parallel to $\hat{n}$. Obtaining fluorescence textures for different polarizations, we extract $\hat{n}$ [13].
[16] R. Podgornik *et al.*, Biophys. Chem. **57**, 111 (1995).
[17] F. Livolant and A. Leforeestier, Prog. Polym. Sci. **21**, 1115 (1996).
[18] H. H. Strey, V. A. Parsegian, and R. Podgornik, Phys. Rev. E **59**, 999 (1999).
[19] J. V. Selinger and R. F. Bruinsma, Phys. Rev. A **43**, 2910 (1991); **43**, 2922 (1991).
[20] P. G. de Gennes, Mol. Cryst. Liq. Cryst. **34**, 177 (1977).
[21] A. Ciferri, W. R. Krigbaum, and R. B. Meyer, *Polymer Liquid Crystals* (Academic, New York, 1982).
[22] Using FCPM and fluorescence imaging of single dyed DNA within unlabeled DNA molecules, we found that both the droplet-air interface and the solid substrates impose tangential boundary conditions on $\hat{n}$ at the interfaces. This implies that the surface anchoring energy is minimized for tangential $\hat{n}$ (consistent with Meyer's entropy considerations for long chains at the surfaces with no chemical binding [21]). DNA orientation at the air interface was additionally confirmed by visualizing $\hat{n}$ structures around air bubbles injected into the DNA LC.
[23] O. Zribi *et al.* (to be published).
[24] N. Morii *et al.*, Biomacromolecules **5**, 2297 (2004); Biopolymers **77**, 163 (2005).
[25] T. Okubo and K. Koboyashi, J. Colloid Interface Sci. **205**, 433 (1998).
[26] R. D. Deegan, Phys. Rev. E **61**, 475 (2000); V. N. Truskett and K. J. Stebe, Langmuir **19**, 8271 (2003); Phys. Rev. Lett. **88**, 164501 (2002).
[27] H. Yokota *et al.*, Nucleic Acids Res. **25**, 1064 (1997).
[28] P. Oswald *et al.*, J. Phys. II (France) **6**, 281 (1996).
[29] L. Vonna *et al.*, Langmuir **21**, 9635 (2005).
[30] R. G. Larson, J. Rheol. (N.Y.) **37**, 175 (1993); F. Livolant, J. Phys. (Paris) **48**, 1051 (1987).